ROTATING ELECTROMAGNETIC FIELD FOR NDT INSPECTIONS

M. Cacciola, D. Pellicanó, G. Megali, S. Calcagno and F. C. Morabito

DIMET Department
University "Mediterranea" of Reggio Calabria
Via Graziella, Feo di Vito, I-89100 Reggio Calabria, Italy

Abstract—Reliable performance of a component or structure depends on its pre-service quality and in-service degradation under operating conditions. The importance of Non-Destructive Testing and Evaluation is ever increasing, above all in ensuring pre-service quality and monitoring in-service degradation, in order to avoid premature failure of the components/structures. There are many Non-Destructive Techniques based on various physical principles. In this work, our main objective is the characterization of anomalies such as defects, stresses and microstructural degradations in materials. Particularly, in this work we propose a Finite Element Method based approach for modelling a fast and accurate evaluation of defects in metallic materials able to easily detect defects, aside from the orientation. Within this framework, the paper proposes the application of a magnetic field rotating perpendicularly to the analysed specimen. We discuss a few case studies, starting from numerical simulations and finally highlighting the importance of this approach in order to evaluate the structural integrity assessment.

1. INTRODUCTION

Quality is the foundation of all industry fields. Non-Destructive Testing (NDT) technologies assure the quality, and support the industrial infrastructures. As technology innovation has produced highly-advanced and complicated products, the needs of NDT have been getting higher for quality assurance purpose. Particularly, the analysis of materials used in industrial and civil applications is an important problem in the state-of-art. If we know the internal state of

---

Corresponding author: M. Cacciola (matteo.cacciola@unirc.it).

a colormaterial before unrepairable damages, we can determine the
life time of the material. Moreover, we can prolong the life time
with an adequate analysis about the state of integrity in order to
improve manufacturing quality and ensure public safety. This work
focuses on the development of NDT technique, which uses remote
field Eddy Currents (ECs) induced by rotating magnetic field [1, 2].
Usually, exploiting EC Techniques (ECTs), the variation of magnetic
field **H**, induced by the variation of eddy currents, is considered to
detect the presence of cracks. Particularly, the normal component of
H, i.e., $\mathbf{H}_\perp$, is measured by suitable sensors, since it is not influenced
by the exciting coils. But, if the crack orientation is vertical to the
longitudinal direction of the sensor, the inspection could be insensitive
to the crack presence. Therefore, a direction insensitive inspection
could be very useful in order to improve the quality of the analysis.
In this way, a Rotating Magnetic Field (RMF) sensor can detect
defects through effects exercised in both the x-axis and y-axis. In
this paper we propose the use of a system able to generate a RMF,
rotating perpendicularly to the inspection plan. Its major advantage
is that it allows detection of defects, regardless of their shape and
orientation without mechanical movements of inspection probe. For
our purposes, a Finite Element Analysis (FEA) code has been exploited
for physical modelling [3, 4]. In order to evaluate the proposed model,
three different problems have been analysed. The former deals with the
detection of defects in railway tracks. The second problem manages
the identification of third-level cracks in anodized rivet. Finally, in
the latter case-of-study, we present the detection of defects in welded
metal joints for civil and industrial applications. All these approaches
requires the geometrical and physical definition of the problems [5].
We verified the magnetic field density [6–8], caused by the presence of
defects, for each applications.

2. PRINCIPLE OF RMF AND FEA APPROACH

The generation of a rotating magnetic field exploits the so called
Ferraris effect [9]. A rotating magnetic field can be constructed
using two orthogonal coils with 90 degrees phase difference in their
AC currents. However, in practice such a system would be supplied
through a three-wire arrangement with unequal currents. This
inequality would cause serious problems in standardization of the
conductor size and so, in order to overcome it, three-phase systems
are used where the three currents are equal in magnitude and have 120
degrees phase difference. Three similar coils having mutual geometrical
angles of 120 degrees will create the rotating magnetic field in this case.

In this way, the density of the eddy current field beneath the sensor can perform 360 degrees rotations without a mechanical rotation of the sensor itself. The problem of analysing a specimen using a RMF by analytical method is rather complex. For this reason a numerical approach is indicated. The numerical technique proposed exploits a Finite Element Method code and the 2D $\mathbf{A} - \Psi$ formulation [10]. In the time-harmonic quasi-static case, Ampère-Maxwell's equation includes the displacement current:

$$\nabla \times \mathbf{H} = \mathbf{J} \tag{1}$$

where $\mathbf{H}$ represents the magnetic field and $\mathbf{J}$ the current density, respectively. If we consider a moving object with velocity $\mathbf{v}$ relative to the reference system, the Lorentz force equation establishes that the force $\mathbf{F}$ per charge q is then given by:

$$\frac{\mathbf{F}}{q} = \mathbf{E} + \mathbf{v} \times \mathbf{B} \tag{2}$$

where $\mathbf{E}$ represents the electric field; $\mathbf{v}$ the instantaneous velocity of the object derived from the expression of the Lorentz force and $\mathbf{B}$ the magnetic induction. Since the object is fixed, $\mathbf{v} = 0$. In a conductive medium, an observer travelling with the geometry sees the current density (considering that σ is the electric conductivity) $\mathbf{J} = \sigma(\mathbf{E} + \mathbf{v} \times \mathbf{B}) + \mathbf{J^e}$; therefore, we can rewrite (1) as follows:

$$\nabla \times \mathbf{H} = \sigma \left(\mathbf{E} + \mathbf{v} \times \mathbf{B} \right) + \mathbf{J^e} \tag{3}$$

where $\mathbf{J^e}$ (A/m^2) is an externally generated current density. Considering, for a transient analysis, the definitions of magnetic vector potential $\mathbf{A}$ and electric scalar potential Ψ, and the constitutive relationship for magnetic field and induction:

$$\mathbf{B} = \nabla \times \mathbf{A} \tag{4}$$

$$\mathbf{E} = -\nabla \Psi - \frac{\partial \mathbf{A}}{\partial t} \tag{5}$$

$$\mathbf{B} = \mu_0 \mu_r \mathbf{H} \Leftrightarrow \mathbf{H} = \mu_0^{-1} \mu_r^{-1} \mathbf{B} \tag{6}$$

where μ_0 and μ_r are free space and relative magnetic permeability; we may rewrite (3), by substituting (4) in it, as:

$$\sigma \frac{\partial \mathbf{A}}{\partial t} + \nabla \times \left(\mu_0^{-1} \mu_r^{-1} \nabla \times \mathbf{A} \right) - \sigma \mathbf{v} \times (\nabla \times \mathbf{A}) + \sigma \nabla \Psi = \mathbf{J^e} \tag{7}$$

Since we are interested in perpendicular induction current, only the z-component of $\mathbf{A}$ is non null. Therefore, the formulation of the 3D Equation (7) is simplified to:

$$\sigma \frac{\partial \mathbf{A}_z}{\partial t} + \nabla \times \left(\mu_0^{-1} \mu_r^{-1} \nabla \times \mathbf{A}_z \right) - \sigma \mathbf{v} \times (\nabla \times \mathbf{A}_z) = \sigma \frac{\Delta \Psi}{L} + \mathbf{J^e}_z \tag{8}$$

where $\Delta\Psi$ is the difference of electric potential and L is the thickness along the z-axis. The Partial Difference Equation (PDE) formulation of Equation (7) can be written as:

$$\sigma\frac{\partial A_z}{\partial t} + \nabla \cdot \left(\mu_0^{-1}\mu_r^{-1}\nabla A_z\right) - \sigma\mathbf{v} \cdot \nabla A_z = \sigma\frac{\Delta\Psi}{L} + J_z^e \qquad (9)$$

In this way, we calculated the magnetic vector potential $\mathbf{A}$ in a generic subdomain Ω. For our aim, it is necessary to impose the boundary conditions as follows. Magnetic field $(\mathbf{n} \times \mathbf{H} = \mathbf{n} \times \mathbf{H_0})$ for boundary of air where acting the RMF; for remaining boundaries, included the defect, the continuity is assured by the expression $\mathbf{n} \times (\mathbf{H_1} - \mathbf{H_2}) = 0$ [11, 12]. The rotation effect of the magnetic field vector has been simulated by applying a uniform $\mathbf{B}$ vector, timely rotated according to the following Euler rotation formulation [15]:

$$\begin{bmatrix} \mathbf{B_x}(t+\tau) \\ \mathbf{B_y}(t+\tau) \end{bmatrix} = \begin{bmatrix} \cos(\omega t) & \sin(\omega t) \\ -\sin(\omega t) & \cos(\omega t) \end{bmatrix} \begin{bmatrix} \mathbf{B_x}(t) \\ \mathbf{B_y}(t) \end{bmatrix} \qquad (10)$$

where ω is the pulse of inducing current.

3. RMF AND ITS APPLICATIONS IN ENGINEERING USING FEA

The principal objective of a RMF based nondestructive examination is to provide the inspector with quantitative as well as qualitative information. This is achieved by detecting, locating and sizing any detected flaws. Several types of defect exist, for example cracks, voids, corrosion, inclusions, delaminations, impact damage and holes. These defects begin as minor flaws which can occur as the result of excessive loading or external stresses applied to a material. If not discovered at an early stage, they may develop into dangerous faults. The goal of this section is to provide a practical knowledge of civil and industrial applications of this approach.

3.1. Case study ♯ 1: RMF for Cracks Detection in Railway Tracks

Safety in railways and tram-ways is one of the key issues of public transportation companies. The state of the tracks is relevant in this perspective, in particular when high-speed trains are envisioned. Frequent monitoring of the tracks is therefore critical to plan and has cost-effective maintenance. Detection of wear and deformation of tracks at an early stage allows for better scheduling of the maintenance, avoiding the need of immediate action when dangerous

conditions are observed. Advanced maintenance planning reduces also costs since the limited human and equipment resources can be better used. Besides, accurate maintenance decreases the acoustic pollution due to bad coupling between wheel and track: This is relevant especially within towns. We propose a FEM-based approach in order to plan the maintenance of railway tracks. It is presently possible to perform forward numerical simulations [1–3] very precisely and rapidly and concerning different applications of NDT. With the evolution of computer systems and numerical methods, the interest in NDT has grown so much that problems, which a few years ago appeared very difficult to be practically solved, can now be approached by numerical simulations. Cracks or other in-service expected discontinuities occurring in railway may lead to fracture and thus to operational danger. Where necessary, operational safety is guaranteed by the periodic non-destructive inspection of these components. Irregularities may not exceed a specified and limited extension. Moreover, irregularities are closely related to operating speed, covering distance, quality of the track, acceleration, profile wear, rail wear, stiffness bogey, and so on. For this reason, the initial inspection shall be exploited in order to observe all discontinuities or damages. Our numerical simulations were carried out according to the requirements and advices of international standards: European standard (EN), International Standard (ISO) and Unit Identification Code (UIC). As the EN or ISO standards approach the acceptance of rolling stock components in manufacturing stage and not directly in-service inspections, a study of UIC documents and experience achieved after 4 years inspections, in railway networks, focus the inspection requirements. The available rolling stock standards concerning NDT are:

- **ISO 1005-1:1994**: Railway rolling stock material — Part 1: Rough-rolled tyres for tractive and trailing stock — Technical delivery conditions;
- **ISO 1005-3:1982**: Railway rolling stock material — Part 3: Axles for tractive and trailing stock — Quality requirements;
- **ISO 1005-6:1994**: Railway rolling stock material — Part 6: Solid wheels for tractive and trailing stock — Technical delivery conditions.

The most common defects in railway are Rolling Contact Fatigue (RCF) cracks, flats and internal cracks initiated from manufacturing defects with diameter less than 1 mm. Thus, we assumed all these indications in our simulations. For our purposes, a FEA code has been exploited for physical modelling [5]. It requires the geometrical

Table 1. Geometrical and physical parameters for simulation step.

Property	Setting
Railway dimensions	$0.14 \times 0.2\,\mathrm{m}$
Electric conductivity	$4.032 \times 10^{6}\,(\mathrm{S/m})$

Table 2. Electrical parameters.

Parameter	Dimension
Frequency	$50\,\mathrm{Hz}$
Pulse	$2\pi f$ (rad/sec)
Magnetic Field	$1 \times 10^{-3}\,(\mathrm{T})$ in magnitude

and physical definition of the railway [6]. Table 1 resumes these settings. We verified the magnetic field density [7, 8] caused by the presence of defect. A suitable database of results has been generated in correlation with the rail and track inspection data. It gives the necessary information about discontinuities created in rail components during specific rail and track conditions. For our purpose we verified the variation of the magnetic field's density caused by the presence of the defect [7, 8]. For our aims we imposed the magnitude of electrical parameters, according to Table 2. The performances shown by the proposed solutions are very encouraging: The use of a rotating magnetic field allows not only to detect defects despite of their orientations, but also increases the ability of detecting very small cracks in railways. In Fig. 1, we depict typical defects (called "A": bottom defect; "B": middle defect and "C": top defect) and their representation of preferential direction for crack evolution. The progression of cracks is inspected with the main electrical parameters previously presented. The dimensional progression of cracks, according to the frequency analysis, is summarized in Table 3. Results have been compared with numerical output of a railway section without defects, inspected with the same electrical parameters. Fig. 2 depicts a comparison between the numerical simulations without effect and with the increase of the different kind of defects. For a complete investigation, we have obtained final graphs of the progression of magnitude and phase of **B** for a frequency value of $50\,\mathrm{Hz}$. For our aims, final graphs show the difference of information obtained on crack's presence or absence. Results demonstrate the accuracy of the developed simulations with the FEA model and its efficacy in the proposed problem.
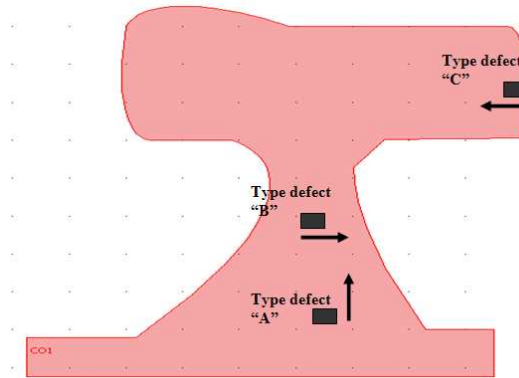
Figure 1. Geometrical representation of the problem and representation of preferential direction for crack evolution.

Table 3. Geometrical parameters imposed in FEA analysis with a frequency of 50 Hz and a magnetic field applied of 1 (mT) in modulus.

Crack type	Height defect	Length defect
A	from 1 to 4 mm	1 mm
B	1 mm	from 1 to 5 mm
C	1 mm	20–60–100 mm

Table 4. Geometrical and physical parameters for FEA-based simulations.

Parameter	Dimension
Wing dimensions	50 mm × 9 mm
Electric wing conductivity	3.774×10^7 (S/m)
Rivet dimensions	4 mm × 6 mm × 9 mm
Electric rivet conductivity	1.9574×10^7 (S/m)

3.2. Case study ♯ 2: RMF for Third-layer Cracks Identification in Aging Aircrafts

Aircrafts due to their massive use, have to bear, during their life cycle, alternating loads of continuous vibrations and shock waves. They cause fatigue cracks, which can be nondestructively inspected by using Eddy Current Testings (ECTs) [13]. ECTs, in fact, are especially sensitive on high conductive materials like aluminium; furthermore, they are not restricted by any safety regulation, and are easy to use
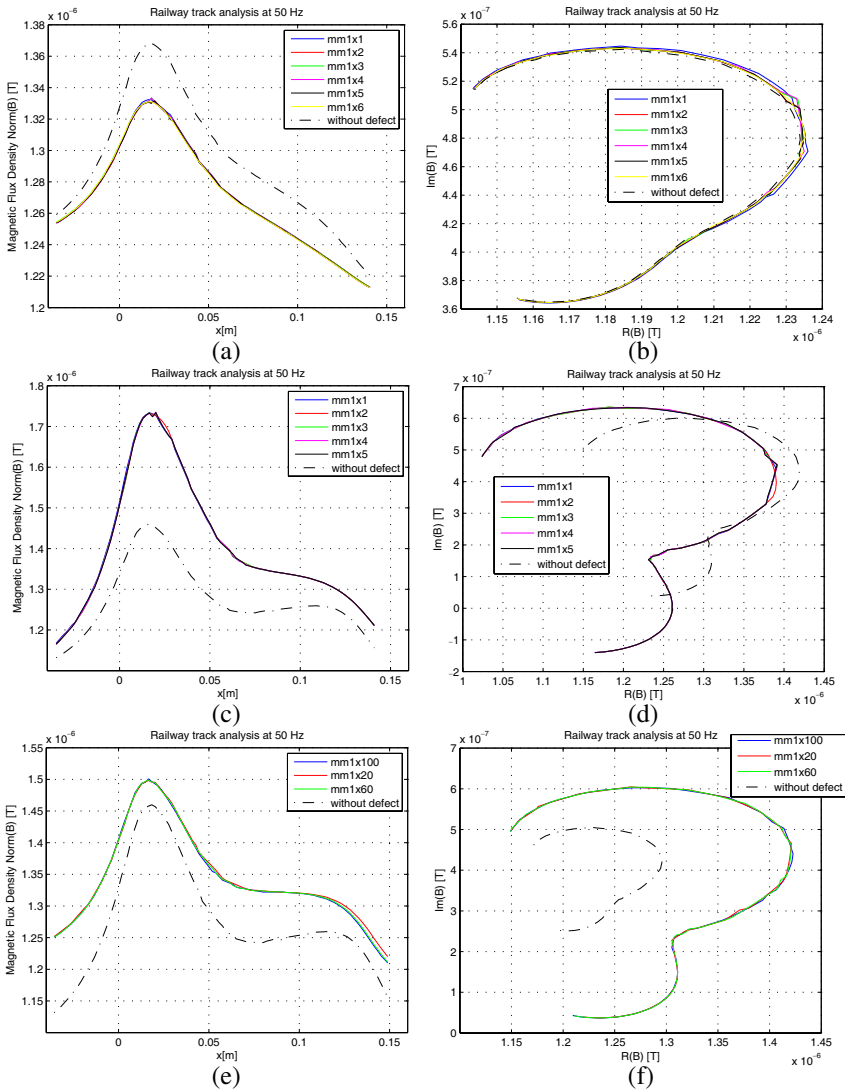
Figure 2. Variation of magnetic field's density module and phase in presence of cracks compared with the railway without defect. (a) Modulus of magnetic flux density "A" type crack. (b) Phase of magnetic flux density "A" type crack. (c) Modulus of magnetic flux density "B" type crack. (d) Phase of magnetic flux density "B" type crack. (e) Modulus of magnetic flux density "C" type crack. (f) Phase of magnetic flux density "C" type crack.

and mechanically robust. However, the sensitivity of ECT systems depends on depth and volume of the damage and the reliability is reduced by disturbing effects. In multi-layered rivet-joint aluminium structures, strong influences on the crack's detection are caused by the rivets [14]. Obviously, the higher the deep of crack, the more difficult its detection. In particular in deeper layers of multi-layered aluminium structures, bending cracks, which don't go through the whole thickness of the layer, are difficult to detect. Table 4 resumes FEA settings. Using cracks' dimensions going from 1×1 mm up up to complete crack and carrying out their inspections, we verified the variation of the magnetic field's density caused by the presence of the defect [15–17]. For determining the final solution, it is necessary to impose the boundary conditions as follows. Magnetic field ($\mathbf{n} \times \mathbf{H} = \mathbf{n} \times \mathbf{H_0}$) for boundary of air where acting the rotating magnetic field; for remaining boundaries, included the defect, the continuity is assured by the expression $\mathbf{n} \times (\mathbf{H_1} - \mathbf{H_2}) = 0$ [18]. For our aims, we imposed the magnitude of electrical parameters according to Table 4, and the magnitude of magnetic field equal to 0.003 T. Fig. 3 shows a representation of the problem; Fig. 4 shows a detail of increasing of crack dimensions and of its direction of extension instead. Our studies have been based on a discrete domain [19] of a number from 18782 to 18964 elements. The number of degree of freedom go from 37631 to 38331. Mesh has been generated with triangular elements and a geometric dimension of 0.05 mm for wing and rivets. Time simulation goes from 18.188 to 18.75 (sec). The performances shown by the proposed solutions are very encouraging: The use of a rotating magnetic field allows not only to detect defects despite of
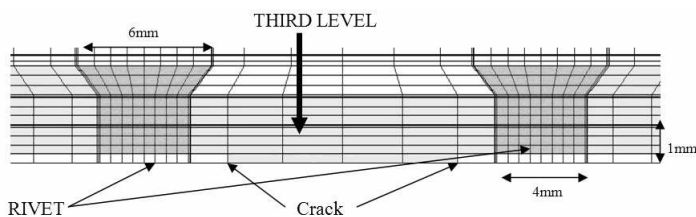
Figure 3. Geometrical representation of problem.

Figure 4. Representation of preferential direction for crack evolution.

their orientations, but also increases the ability of detecting very small third-layer cracks in alodine aluminum rivets.

3.3. Numerical simulations

Numerical simulations have been carried out by our FEA code on a $4 \times 6 \times 9$ mm wing section. The crack evolution under consideration is inspected with the main electrical parameters presented in the previous subsection. The dimensional evolution of cracks goes from 1×1 mm up to complete crack. The frequency of analysis goes from 10 to 50 Hz, with a magnetic field having amplitude 0.003 T. Results have been compared with numerical output of a wing section without defects, inspected changing frequency of rotating magnetic field applied (from 10 to 50 Hz). Fig. 5 depicts a comparison between the numerical simulations without defect and with a defect of 1×1 mm for a frequency of 10 Hz and 50 Hz. Results demonstrate the accuracy of the developed simulations with the FEA model and its efficacy in the proposed problem. The results presented in this section are completed by two 3D plots of wing evaluation, showing the final numerical variations of field's density obtained with a frequency analysis of 50 Hz for a specimen without defect and for the same specimen but with a defect extended from rivet to rivet.

3.4. Case Study ♯ 3: RMF for Cracks Detection in Welded Joints

A typical framework where NDT inspection can be encountered is the welding process, i.e., the application of a joint on two or more pieces. In the welding strip, matter of discontinuity appears at micro-scale as either spherical or elliptical air bubbles. These discontinuities cause a stress concentration, modifying the constitutive response of the material, or, in other words, building a damage within the material. The latter phenomenon represents the initial step to crack extension and, consequently, the voids' detection and control should be investigated by means of reliable devices and procedures. The quality of a welded joint depends on the product allocation. In fact, some types of welding are suitable for a particular case, the same type of welding will not be eligible in another situation. The quality is devised according to the intended use of the joint, but it takes into account all factors that may affect the welding. Scientific literature suggests a lot of different solutions for the problem of material inspection. Nowadays, the mostly used techniques are based on NDT, having a very important role in inspecting aging materials for industrial applications or within the framework of civil engineering.
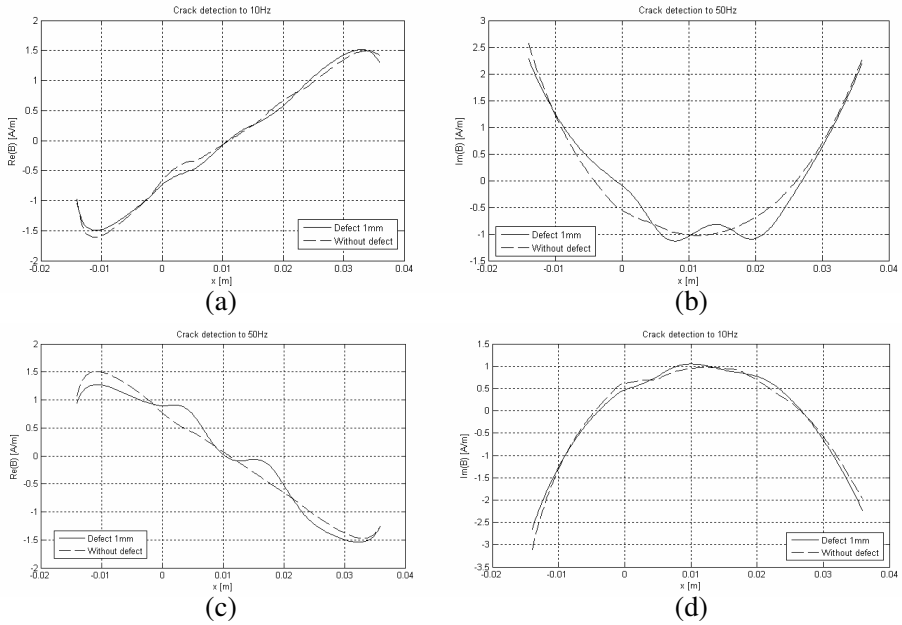
Figure 5. Variation of magnetic field's density. (a) Frequency inspection of 10 Hz — Real part. (b) Frequency inspection of 10 Hz — Imag part. (c) Frequency inspection of 50 Hz — Real part. (d) Frequency inspection of 50 Hz — Imag part.
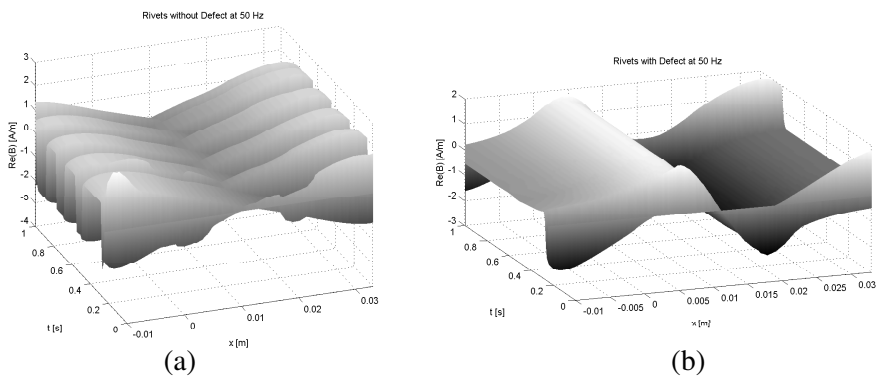
Figure 6. Three-dimensional views of the final result analysis, variation of magnetic field's density. (a) Re($\mathbf{B}$) without defect. (b) Re($\mathbf{B}$) with defect.

3.4.1. An Overview of Defectiveness in Welding Strips

Welding process could induce the following relevant defects, compromising the structural integrity of the same strips and consequently, of specific components and structures:

- **lack of fusion**: If the fusion of the basic metal is excessive, continue grooves are formed on the sides, causing a depression along the sides of the cord; sometimes the incisions can be eliminated by using a thin covering material;

- **excess of penetration on the top (dripping)**: If a huge quantity of metal is caught at the top of the weld: a toe crack could be determined;

- **incomplete penetration**: It is caused by a lack of fusion at the welding apex, and seriously reduces the resistance of the joint; in heading welding made with one or more rubs, the defect can be eliminated by chiselling out and giving an additional rub;

- **gluing**: It occurs when, during the welding process, the complete fusion of metal does not take place, i.e., when the welding metal overlaps the not-yet-fused material to weld, without a mixing between the metals;

- **cracks**: The most serious kind of flaws, because they originate from phenomena of metallurgical nature. Since they depend on the cracking temperature, they are named as hot or cold cracks.

Figure 7 shows the most typical defects in metal welded strips. Sizes can vary, greatly depending on the welding process and conditions. For instance, according to European laws UNI EN 287-2 and UNI EN 288-4, the maximum tolerable crack dimension is fixed to 0.5 mm of diameter for a circular defect. The geometry of the examined case presents a "V" type welding, where a bubble shaped defect has been modelled. Geometrical dimensions and electrical parameters of our model are listed in Table 5 and Table 6, numerical results are shown in Fig. 8.
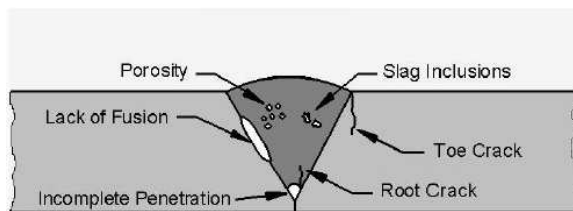
Figure 7. Categories of discontinuity in metal welded strips.

Table 5. General settings of numerical models.

Property	Setting
Specimen material	Stainless steel, not-magnetic, Isotropic
Dimension of specimen	$0.2\,\mathrm{m} \times 0.01\,\mathrm{m}$
Welding thickness	$0.02\,\mathrm{m}$
Min. diameter of the defect	$0.5\,\mathrm{mm}$
Max. diameter of the defect	$1\,\mathrm{mm}$

Table 6. Electrical parameters.

Parameter	Dimension
Frequency	from 10 to $50\,\mathrm{Hz}$
Specimen conductivity	$4.032 \times 106\,(\mathrm{S/m})$
Pulse	$2\pi f\ (\mathrm{rad/sec})$
Magnetic Field	$3 \times 10^{-3}\,\mathrm{T}$ in magnitude
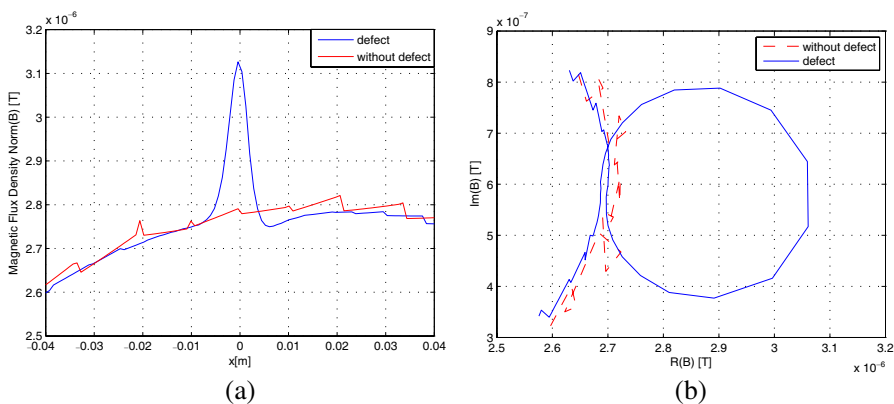
Figure 8. Variation of magnetic field's density module and phase in presence of crack respect the weld without defect. (a) Modulus of magnetic flux density. (b) Phase of magnetic flux density.

4. CONCLUSION

By using the numerical method presented in this paper, we developed finite element procedures for the evaluation of the rotating magnetic field in NDT inspections. This procedure has been applied in three different case study: Defect detection in railway tracks, third-layer cracks identification in aging aircrafts and cracks detection in welded

joints. For our analysis, we used 2D sections of geometries according to the ISO rules. Specifically, exploiting the Ferraris effect, 2D time dependent models have been studied to evaluate the distortion of the magnetic field density due to the defect presence: RMF provides a good overall accuracy in discriminating defect presence, as our experimentations demonstrate. At the same time, the procedure should be validate for other kind of defects, with different geometries or orientations. The same approach should find useful applications like: Detection of third-layer cracks, above all concerning alodine rivets within the framework of aging aircrafts' inspection, or micro-crack and micro-voids detection in welding process. Anyway, the presented results, which also can be considered as preliminary results, are very encouraging and they suggest the possibility of increasing and generalizing the performance model with a physical realization of a rotating field eddy current sensor. Within this framework, experimentations are required in order to verify the real effects of the proposed method as well as to certify the accuracy of the measurement system. The authors are actually engaged in this direction.

REFERENCES

1. Grimberg, R., I. Olteanu, T. Cristea, M. Goia, D. Gradinariu, R. Plavanescu, T. Bacanu, A. Andreescu, and D. Apavaloaie, "Eddy current examination of steel wires," *NDT Int.*, Vol. 23, No. 4, 201, 1990.

2. Grimberg, R., A. Savin, O. Mihalache, N. Rezlescu, E. Bradu, S. Chifan, V. Iftimi, and A. Andreescu, "Reliability of automatic eddy-current equipment with a rotating magnetic field," *NDT and E International*, Vol. 28, No. 5, 297–301, 1995.

3. Tagaki, T., H. Huang, H. Fukutomi, and J. Tani, "Numerical evaluation of correlation between crack size and eddy current testing signals by a very fast simulator," *IEEE Transactions on Magnetics*, Vol. 34, 2582–2584, 1998.

4. Nevels, R., J. Miller, and J. Miller, "Rotation in electromagnetic field equations: A discussion, interpretation and application," *IEEE Transactions on Magnetics*, Vol. 2, 875–878, 1998.

5. Specogna, S. and F. Trevisan, "Voltage Driven coils within a discrete geometric approach to 3D eddy-currents," *Proceedings of 11th IGTE Symposium on Numerical Fields Calculation*, 81–84, 2004.

6. Tonti, E., "Algebric topology and computational electromag-

netism," *Proceedings 4th Int. Workshop Electric Magnetic Fields*, 284–294, 1998.

7. Dodd, C. V. and W. E. Deeds, "Analytical solutions to eddy-current probe-coil problems," *J. Appl. Phys.*, Vol. 39, 2829–2838, 1968.

8. Lewis, A. M., "A theoretical model of the response of an eddy-current probe to a surface-breaking metal fatigue crack in a flat test piece," *J. Phys. D: Appl. Phys.*, Vol. 25, 319–326, 1992.

9. Ferraris, G., "Rotazioni elettrodinamiche prodotte per mezzo di correnti alternate," , *Atti dell'Accademia delle Scienze di Torino*, Vol. 23, 360, 1888 (in Italian).

10. Rodger, D., P. J. Leonard, and H. C. Lai, "Interfacing the general 3D A-ψ method with a thin sheet conductor model," *IEEE Transactions on Magnetics*, Vol. 28, No. 2, 1115–1117, 1992.

11. Tsuboi, H. and T. Misaki, "Three dimensional analysis of eddy current distribution by the boundary element method using vector variables," *IEEE Transactions on Magnetics*, Vol. 23, 3044–3046, 1987.

12. Weissenburger, W. D. and U. R. Christensen, "A network mesh method to calculate eddy currents on conducting surfaces," *IEEE Transactions on Magnetics*, Vol. 18, No. 2, 422–425, 1982.

13. Tober, G. and T. Meier, "Corrosion inspection in aircraft construction," *Zeitschrift Materials and Corrosion*, Vol. 46, 405–409, 1995.

14. Bischoff, W., H.-A. Crostack, and M. Maass, "CS-pulsed eddy current inspection for cracks in multi-layered joint al-alloy aircraft structures," *The E-Journal of Nondestructive Testing & Ultrasonics*, Vol. 3, No. 9, 1998, available online at http://www.ndt.net/article/ecndt98/aero/055/055.htm, January 31st, 2008.

15. Weisteinn, W., "Euler angles," *MathWorld, A Wolfram Web Resource*, available online: http://mathworld.wolfram.com/EulerAngles.html.

16. Dodd, C. V. and W. E. Deeds, "Analytical solutions to eddy-current probe-coil problems," *Journal of Applied Physics*, Vol. 39, 2829–2838, 1968.

17. Lewis, A. M., "A theoretical model of the response of an eddy-current probe to a surface-breaking metal fatigue crack in a flat test piece," *NDT and E International*, Vol. 25, 319–326, 1992.

18. Tsuboi, H. and T. Misaki, "Three dimensional analysis of eddy current distribution by the boundary element method using vector variables," *IEEE Transactions on Magnetics*, Vol. 26, No. 2, 454–

457, 1990.

19. Weissenburger, D. W. and U. R. Christensen, "A network mesh method to calculate eddy currents on conducting surfaces," *IEEE Transaction on Magnetics*, Vol. 18, No. 2, 422–425, 1982.